Journal of Catalysis **193,** 224–237 (2000)
doi:10.1006/jcat.2000.2891, available online at http://www.idealibrary.com on IDEAL®

Lumped Kinetics for Solid-Catalyzed Wet Oxidation: A Versatile Model

Khaled Belkacemi,* Faïçal Larachi,†,[1] and Abdelhamid Sayari†

*Department of Food Sciences & Nutrition and †Department of Chemical Engineering & CERPIC, Laval University, Québec, Canada G1K 7P4

Received November 23, 1999; revised April 3, 2000; accepted April 10, 2000

Kinetic modeling of solid-catalyzed deep oxidation of pollutants in water is crucial to the design and scale-up of wastewater wet oxidation treatment. Due to their simplicity, the overall kinetics using power-law rates are often unable to capture the important features in such oxidation systems. However, detailed mechanistic approaches aimed at establishing complex reaction networks where several species and intermediates need to be identified become quickly cumbersome and costly. Lumped kinetic approaches offer a balanced trade-off between sophistication and simplicity. A versatile "three-lump" triangular kinetic model was proposed for the description of solid-catalyzed wet oxidation of various pollutants in wastewater effluents. The model is an offshoot of the well-known "generalized lumped kinetic model" introduced for homogeneous wet oxidation. This model was extended, using the Langmuir–Hinshelwood–Hougen–Watson framework, to describe the evolution of heterogeneous catalytic wet oxidation reactions. The model, in the form of a set of three implicit nonlinear differential equations, was validated using literature data obtained under a variety of experimental conditions, such as subcritical or supercritical water conditions, batch and continuous reactors, a multitude of organic loads in the form of carbon-, nitrogen-, and oxygen-bearing compounds, and using different kinetic variables such as TOC and COD. In all cases, this strategy led to calculated parameters that met the thermodynamic, kinetic, and statistical criteria. The uncertainty and confidence joint regions were estimated using bootstrap "Monte Carlo" techniques.

Key Words: **heterogeneous wet oxidation; lumped kinetics; detoxification; wastewater.**

INTRODUCTION

Water is an increasingly coveted commodity. As a result, regional and planetary policies are being implemented for the effective and parsimonious exploitation of water resources. Nevertheless, the management of toxic and hazardous wastewater streams is still a perennial problem facing industries, governments, and environmental and health protection agencies. Due to the increasingly rigorous quality control of effluents, the manufacturing industries have to minimize waste in the first place using efficient routes via the so-called "atom economy" concept, i.e., maximization of atom utilization, from raw materials to final products (1, 2). In addition, it is vital to develop highly efficient processes capable of destroying hazardous xenobiotic pollutants in "end-of-pipe" waste effluents.

Wastewater effluents that are too dilute to incinerate and yet too toxic to bio-treat can suitably be dealt with by (solid-) catalyzed wet oxidation (CWO). The recourse to solid catalysts offers a suitable technological alternative to the conventional noncatalytic or homogeneously catalyzed routes not only because the treatment takes place under much milder conditions but also because the catalyst may be easily recovered and reused. Hence CWO is so versatile that wastewaters containing a range of organic and/or inorganic pollutants, including carbon (C)-, oxygen (O)-, nitrogen (N)-, halogen (X)-, sulfur (S)-, and phosphorus (P)-bearing molecules, are being tackled efficiently. Oxidative degradation of such compounds involves a myriad of successive and simultaneous reactions. This makes it unrealistic to envisage comprehensive CWO kinetic studies based on exhaustive mechanistic considerations. At the other extreme, overall power-law kinetic rate approaches are often too simple to adequately describe the CWO of complex mixtures. The lumped kinetics approach (LKA), which is widely used in petrochemistry (3), often offers a suitable trade-off between tedious mechanistic/kinetic formalisms and oversimplified power-law representations. For reactor design and scale-up considerations, the LKA is by far the most useful strategy when dealing with the kinetics of reactions with complex mixtures such as waste-waters (4).

Thus far, the phenomenological taxonomy of LKA proposed through the so-called "generalized lumped kinetic model" (GLKM) (5) appears to be the most successful approach to the *noncatalytic* wet oxidation of pure or mixed organic species (3). The "three-lump" GLKM simplified scheme, shown below, postulates that as the reaction proceeds, all the species can be pruned within three characteristic lumps, namely,

- lump A for parent compounds and unstable organic intermediates, except acetic acid,
- lump B for refractory intermediates, acetic acid being a typical representative, and
- lump C for oxidation end-products.

[1] To whom correspondence should be addressed. E-mail: flarachi@gch.ulaval.ca.

0021-9517/00 $35.00

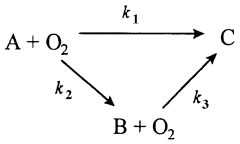

Other LKA taxonomies akin to the GKLM were also successfully applied in several earlier studies on noncatalytic wet oxidation (6–8).

Since kinetic rate equations for heterogeneously catalyzed reactions are based on the same laws of chemical kinetics as those applied to homogeneous processes, attempts were made to use the GLKM in the context of CWO (9, 10). Unfortunately, the specificity of solid-catalyzed reactions reflected in the surface reaction and the adsorption and desorption of lumps has been overlooked. This resulted in kinetic constants violating the Arrhenius equation, while sometimes negative activation energies were obtained. To address these shortcomings, Zhang and Chuang (11) reduced the GLKM structure to a three-lump "two-parallel" scheme, called the lumped kinetic model (LKM), in which no further transformations of B-type lumps take place.

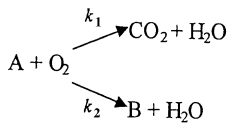

Note that though referred to as intermediates, the B-type lump represents "partial-oxidation" *end products*. Here again, specific features of solid-catalyzed reactions were not incorporated in the model. Furthermore, this picture may not be realistic since the occurrence of *infinitely* refractory (or anti-oxidative) B-lump molecules has not yet been proven experimentally.

The objective of this article is to provide a rigorous lumped kinetics framework for *solid-catalyzed* wet oxidation reactions and to introduce statistical techniques for the estimation of parameter confidence intervals. The model recasts the GLKM (5) within the framework of Langmuir–Hinshelwood–Hougen–Watson (LHHW) wherein surface reactions, adsorption, and desorption steps for each lump are accounted for. The versatility of the model is illustrated using literature data dealing with a large variety of pollutants and a wide range of conditions, e.g., sub- and supercritical wet oxidation, batch and flow-through kinetic reactors, and single- and multiple-pollutant effluents. The selected examples also use different properties such as TOC, COD, or TN to monitor the evolution of CWO.

A LUMPED KINETIC MODEL FOR CWO

The LHHW approach is proposed to circumvent the setbacks encountered when reaction kinetic schemes devised for homogeneous reactions are applied to heterogeneous processes. To extend the reaction pathway governing the GLKM (5) to solid-catalyzed wet oxidation, it is required that we include additional physical and chemical steps to describe reactant and/or product adsorption/desorption as well as surface reactions. The reaction pathway may be envisioned as follows: lump A species adsorb on the catalyst surface, undergo surface reactions into adsorbed intermediate (lump B), then into end product (lump C); both may desorb and leave the catalyst surface. The general reaction scheme, depicted by a sequence of elementary steps according to the LHHW approach, is illustrated in Fig. 1. Hereafter, the GLKM model extended to CWO will be referred to as the "extended lumped kinetic model" or the ELKM. Also, for the ELKM to be applicable to wastewaters containing hetero-atom compounds, the three lumps were defined in very general terms as follows:

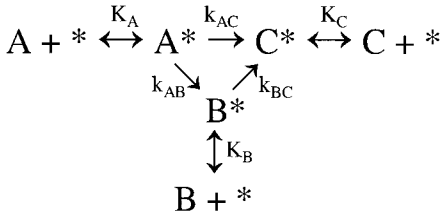

FIG. 1. Network reaction pathway for heterogeneously catalyzed wet oxidation.

- lump A designates the parent water-dissolved compounds;
- lump B encompasses all soluble intermediates produced by CWO, including the stable ones;
- lump C represents all gaseous and solid end products.

The following assumptions were made to establish the ELKM set of equations:

(i) Surface reactions of chemisorbed pseudo-species (A^*), intermediate (B^*), and product (C^*) are rate controlling compared to the adsorption/desorption steps. This can be stated in terms of relative magnitudes of the rate constants:

$$k_{AB}, k_{AC}, k_{BC} \ll k_A, k_{-A}, k_B, k_{-B}, k_C, k_{-C}. \qquad [1]$$

(ii) All sites ($*$) whereon surface reactions occur are identical.

(iii) All elementary steps involve partial first order relative to their respective reactants.

(iv) Usually far in excess of the stoichiometric ratio, O_2 concentration is assumed constant.

(v) Mass transfer interfacial limitations and intraparticle resistance are neglected.

(vi) No irreversible loss of active sites occurs.

Let X_0, X, X^*_A, X^*_B, X^*_C be the concentrations of initial active sites, actual free active sites, and sites occupied by A, B, and C lumps, respectively. The overall reaction pathway, shown in Fig. 1, can be broken down into the following series of elementary steps.

I. $A + * \overset{K_A}{\longleftrightarrow} A^* \Rightarrow$ Adsorption of A

II. $B^* \overset{K_B}{\longleftrightarrow} B + * \Rightarrow$ Desorption of B

III. $C^* \overset{K_C}{\longleftrightarrow} C + * \Rightarrow$ Desorption of C

IV. $A^* \overset{k_{AB}}{\longrightarrow} B^* \Rightarrow$ Surface reaction

V. $A^* \overset{k_{AC}}{\longrightarrow} C^* \Rightarrow$ Surface reaction

VI. $B^* \overset{k_{BC}}{\longrightarrow} C^* \Rightarrow$ Surface reaction

From steps I–III, we have

$$X^*_A = K_A X C_A \quad [2]$$

$$X^*_B = K_B X C_B \quad [3]$$

$$X^*_C = K_C X C_C. \quad [4]$$

Assumption (i) leads to

$$R_A \cong -(k_{AB} + k_{AC}) X^*_A \quad [5]$$

$$R_B \cong k_{AB} X^*_A - k_{BC} X^*_B \quad [6]$$

$$R_C \cong k_{AC} X^*_A + k_{BC} X^*_B. \quad [7]$$

From assumption (vi) the site balance is

$$X_0 = X + X^*_A + X^*_B + X^*_C. \quad [8]$$

Combination of Eqs. [2]–[4] and [8] leads to

$$X = \frac{X_0}{1 + K_A C_A + K_B C_B + K_C C_C}. \quad [9]$$

Combining and rearranging Eqs. [2]–[9], the rate of consumption of A lumps (R_A), evolution of B lumps (R_B), and formation of C lumps (R_C) can be written as

$$R_A \cong -\frac{(\tilde{k}_{AB} + \tilde{k}_{AC}) K_A C_A}{1 + K_A C_A + K_B C_B + K_C C_C} \quad [10]$$

$$R_B \cong \frac{\tilde{k}_{AB} K_A C_A - \tilde{k}_{BC} K_B C_B}{1 + K_A C_A + K_B C_B + K_C C_C} \quad [11]$$

$$R_C \cong \frac{\tilde{k}_{AC} K_A C_A + \tilde{k}_{BC} K_B C_B}{1 + K_A C_A + K_B C_B + K_C C_C}, \quad [12]$$

where the total active site concentration X_0, being nonmeasurable, was embedded into the rate constants of elementary steps IV–VI:

$$\tilde{k}_{AB} = k_{AB} X_0; \quad \tilde{k}_{AC} = k_{AC} X_0; \quad \tilde{k}_{BC} = k_{BC} X_0. \quad [13]$$

For either a perfectly stirred liquid-batch transient reactor or a steady-state liquid-plug flow continuous fixed-bed reactor with a constant fluid streamwise velocity, the ELKM writes

$$\frac{dC_A}{dt\,(\text{or}\,d\tau)} = -\frac{m_{cat}(\tilde{k}_{AB} + \tilde{k}_{AC}) K_A C_A}{1 + K_A C_A + K_B C_B + K_C C_C} \quad [14]$$

$$\frac{dC_B}{dt\,(\text{or}\,d\tau)} = \frac{m_{cat}(\tilde{k}_{AB} K_A C_A - \tilde{k}_{BC} K_B C_B)}{1 + K_A C_A + K_B C_B + K_C C_C} \quad [15]$$

$$\frac{dC_C}{dt\,(\text{or}\,d\tau)} = \frac{m_{cat}(\tilde{k}_{AC} K_A C_A + \tilde{k}_{BC} K_B C_B)}{1 + K_A C_A + K_B C_B + K_C C_C} \quad [16]$$

subject to the initial/boundary conditions

$$C_A = C_{Ao}, \quad C_B = 0, \quad C_c = 0 \;@\; t\,(\text{or}\;\tau = z/U_L) = 0. \quad [17]$$

ELKM LUMPS, SELECTION AND PARAMETERS

Often, only one characteristic of the reaction system is monitored as a function of (residence) time. This characteristic may be "chemical oxygen demand" (COD), "total organic carbon" (TOC), "total nitrogen" (TN), and so forth. Accordingly, the ELKM will use only one such characteristic at a time. The way of defining the lumps depends on the characteristics being monitored (Fig. 2). For example,

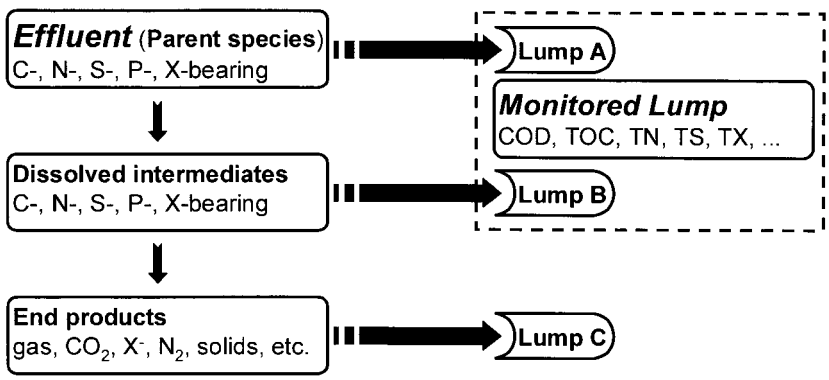

FIG. 2. Taxonomy of lumped kinetics and ELKM species into the CWO monitored variables.

when using TOC, A, B, and C are expressed as

$$\mathrm{TOC} = C_\mathrm{A} + C_\mathrm{B}, \quad \text{and} \quad C_\mathrm{C} = \mathrm{TOC}_0 - \mathrm{TOC}. \quad [18]$$

For the proposed ELKM, the parameters vector to be determined is $\underline{\theta} = [\tilde{k}_{AB}, \tilde{k}_{BC}, \tilde{k}_{AC}, K_A, K_B, K_C]$. Parameter identification rests on solving the least-squares problem U by minimizing the "unweighted least-squares" criterion $\chi^2(\underline{\theta})$,

$$U \begin{cases} \chi^2(\underline{\theta}) = \sum_{i=1}^{n} \sum_{j=1}^{m} (\bar{Y}_{ij} - Y_{ij})^2 \\ \tilde{k}_{AB}, \tilde{k}_{AC}, \tilde{k}_{BC}, K_A, K_B, K_C \geq 0, \end{cases} \quad [19]$$

where Y_{ij} is the jth ELKM state variable from the ith experimental run in the kinetic data set $P = \{P_i, i = 1, n;\ P_i \in \Re^n\}$. The bar stands for the model-predicted quantities. The $\underline{\theta}$ vector was estimated by combining a Runge–Kutta integration algorithm RKS4 (12) with the quasi-Newton constrained optimization method using a mixed quadratic and cubic line search procedure (Matlab Software from MathWorks Inc.)

BOOTSTRAP ESTIMATION OF CONFIDENCE INTERVALS

Direct evaluation of ELKM parameter confidence intervals is impossible due to the implicit and nonlinear nature of the model. In addition, the kinetic data reported in the literature are seldom replicated. This usually impedes direct estimation of parameter confidence intervals. Nonetheless, it is still possible to perform confidence interval assessments using the so-called "bootstrap" Monte Carlo method (13). Hence, B bootstrap sets P_b^* $1 \leq b \leq \mathrm{B}$, of the same size n, are randomly and equiprobably generated from the original experimental kinetic data set P. Each set P_b^* is a resampled version of set P such that P_b^* may contain some repetitive elements from P. From each set P_b^*, an estimate $\underline{\tilde{\theta}}^*$ is evaluated as a bootstrap replication of $\underline{\tilde{\theta}}$ by solving the least-squares problem U. With a reasonably high number of bootstrap replications, a bootstrap estimate of the standard deviation, $\sigma(\tilde{\theta}_i)$; $i = 1, p$, for each ELKM parameter can be evaluated (14),

$$\sigma(\tilde{\theta}_i) = \lim_{B \to \infty} \sqrt{\left(\sum_{b=1}^{B} (\tilde{\theta}_{ib}^* - \langle \tilde{\theta}_i \rangle)^2 / (B-1) \right)}, \quad [20]$$

where

$$\langle \tilde{\theta}_i^* \rangle = \left(\sum_{b=1}^{B} \tilde{\theta}_{ib}^* / B \right). \quad [21]$$

Based on the normality assumption, the confidence limits on ELKM parameters are

$$\tilde{\theta}_i \pm \sigma(\tilde{\theta}_i) t_{B-1,\alpha/2}, \quad [22]$$

where $t_{B-1,\alpha/2}$ is the upper $\alpha/2$ percentile for the student-t variable with $(B-1)$ degrees of freedom.

In addition to parameter standard deviations, complete information on parameter estimation includes evaluation of parameter cross-correlations and determination of joint-confidence regions. Joint-confidence regions are calculated by means of the covariance matrix of $\underline{\tilde{\theta}}^*$

$$\underline{\underline{\mathrm{M}}} = \frac{1}{B-1} \sum_{b=1}^{B} (\underline{\tilde{\theta}}_b^* - \langle \underline{\tilde{\theta}} \rangle)(\underline{\tilde{\theta}}_b^* - \langle \underline{\tilde{\theta}} \rangle)^t, \quad [23]$$

from which the correlation matrix can be computed:

$$\underline{\underline{\Omega}} = \begin{cases} \Omega_{ii} = 1 \\ \Omega_{ij} = \frac{\mathrm{cov}(\tilde{\theta}_i, \tilde{\theta}_j)}{\sigma(\tilde{\theta}_i)\sigma(\tilde{\theta}_j)} \quad \text{if } i \neq j. \end{cases} \quad [24]$$

THERMODYNAMIC CONSTRAINTS

The ELKM parameter vector $\underline{\theta}$ estimated by the least-squares problem U consists of three rate constants, $\tilde{k}_{AB}$, $\tilde{k}_{BC}, \tilde{k}_{AC}$, and three adsorption equilibrium constants, K_A, K_B, K_C. Each rate constant must be consistent with the Arrhenius law,

$$\ln \tilde{k}_i = \ln \tilde{k}_{io} - \frac{E}{RT}, \quad [25]$$

where $\tilde{k}_{io}$ and E should be positive. Also, each adsorption equilibrium constant must be consistent with Van't Hoff relationship

$$\ln K_i = \frac{\Delta S_i}{R} - \frac{\Delta H_i}{RT}. \quad [26]$$

To be thermodynamically consistent, the derived kinetic adsorption coefficients in terms of adsorption enthalpy ΔH and entropy ΔS have to meet the Boudart–Mears–Vannice chemical-kinetic criteria (15)

$$\begin{gathered} \Delta S < 0 \\ 10 < -\Delta S < 12.2 - 0.0014 \Delta H. \end{gathered} \quad [27]$$

Since the adsorption equilibrium constant decreases as temperature is increased for exothermic chemisorption processes, this requires

$$\Delta H < 0. \quad [28]$$

χ^2 FIT OF ARRHENIUS AND VAN'T HOFF RELATIONSHIPS

The χ^2 fits of Eqs. [25] and [26] give the values of ΔH, ΔS, $\tilde{k}_{io}$, and E from the estimated parameters vector $\underline{\theta}$. For the adsorption equilibrium constant K_A this can be

written as

$$\chi^2(\Delta S_A, \Delta H_A; K_A) = \sum_{l=1}^{L} \frac{\left(\ln K_{Al} - \Delta S_{Al} R^{-1} + \Delta H_A R^{-1} T_l^{-1}\right)^2}{\sigma^2_{\ln K_{Al}}}. \quad [29]$$

Similar equations hold for the other rate and equilibrium constants.

The standard deviations in estimated frequency factors, activation energies, and enthalpies and entropies of adsorption for the six steps, i.e., σ_{Ei}, σ_{koi}, $\sigma_{\Delta Hi}$, $\sigma_{\Delta Si}$, are obtained using the bootstrap standard deviations of $\tilde{k}_i$ and K_i (Eq. [20]).

DISCUSSION

Curve Fitting and ELKM Goodness of Fit

At this stage, it may be argued that the current six-parameter ELKM is an "over-parameterized" representation of CWO kinetic data. In other words, there may be other, simpler models requiring fewer kinetic parameters that could account for the experimental data as accurately as the ELKM. To assess this contention, we defined five classes of scenarios corresponding to CWO kinetic models with fitting parameters ranging from 2 (class I) to 6 (class V). For discrimination of the best model, it would be redhibitory to track down scrupulously the formidable number of models arising from the numerous combinations of controlling steps in a six-species scheme, i.e., A, B, C, A*, B*, and C*. Rather, we made the arbitrary but reasonable choice that within each class, we retain for testing only one representative candidate scenario wherein all surface and (fluid) bulk chemical reactions are the sole rate-determining steps. Listed in Table 1 are these representative models with two to six parameters:

- *Class I models*: With the assumption $K_A = K_B = K_C = \tilde{k}_{BC} = 0$, the ELKM degenerates to the two-parameter LKM (11).
- *Class II models*: With $K_A = K_B = K_C = 0$, the ELKM becomes a three-parameter GLKM (5).
- *Class III models*: Considering $K_B = K_C = 0$ leads to a four-parameter CWO model (Table 1).
- *Class IV models*: If $K_C = 0$, the ELKM degenerates to a five-parameter model (Table 1).
- *Class V models*: These models are represented by the six-parameter ELKM, Eqs. [14]–[16].

Likewise, a least-squares problem U similar to that given by Eq. [19] can be performed for each one of the above classes of models. The *likeliness* of the physical steps involved in the assumed pathway for each model was evaluated using the Boudart–Mears–Vannice rules (15) for the adsorption and activation parameters (Eqs. [25]–[28]).

TABLE 1

Discrimination of Five Classes of CWO Kinetic Scenarios: Only Models with Chemical-Reaction Controlling Steps

Reaction scheme	Rate equations and candidate kinetic model	Number of adjustable parameters
Class I		
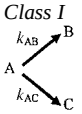	homogeneous (LKM, Ref. (11)) $dC_A/dt = -(k_{AB} + k_{AC})C_A$ $dC_B/dt = k_{AB}C_A$; $dC_C/dt = k_{AC}C_A$	2
Class II		
	homogeneous (GLKM, Ref. (5)) $dC_A/dt = -(k_{AB} + k_{AC})C_A$ $dC_B/dt = k_{AB}C_A - k_{BC}C_B$; $dC_C/dt = k_{AC}C_A + k_{BC}C_B$	3
Class III		
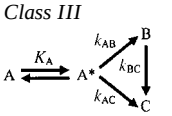	mixed (homo) heterogeneous $dC_A/dt = -m_{cat}(\tilde{k}_{AB} + \tilde{k}_{AC})K_A C_A(1 + K_A C_A)^{-1}$ $dC_B/dt = m_{cat}\tilde{k}_{AB}K_A C_A(1 + K_A C_A)^{-1} - k_{BC}C_B$ $dC_C/dt = m_{cat}\tilde{k}_{AC}K_A C_A(1 + K_A C_A)^{-1} + k_{BC}C_B$	4
Class IV		
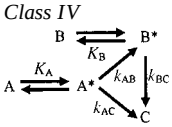	heterogeneous $dC_A/dt = -m_{cat}(\tilde{k}_{AB} + \tilde{k}_{AC})K_A C_A(1 + K_A C_A + K_B C_B)^{-1}$ $dC_B/dt = m_{cat}(\tilde{k}_{AB}K_A C_A - \tilde{k}_{BC}K_B C_B)(1 + K_A C_A + K_B C_B)^{-1}$ $dC_C/dt = m_{cat}(\tilde{k}_{AC}K_A C_A + \tilde{k}_{BC}K_B C_B)(1 + K_A C_A + K_B C_B)^{-1}$	5
Class V		
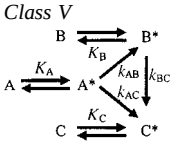	heterogeneous (ELKM, this work) Eqs. [14]–[16]	6

Hence, a likely model must be associated with positive values of activation energies, and as for thermodynamic consistency, negative values for the enthalpy and entropy of adsorption are to be expected.

Concomitantly, the *quality* of the curve fitting for each model must be judged from the values of $\chi^2(\underline{\theta})$ and $Q(\chi^2 \mid \nu = n \times m - p)$ functions, where n is the number of runs, m is the number of monitored observable variables, p is the number of fitted parameters, and ν is the number of degrees of freedom. The use of these statistical criteria is discussed in details in Refs. (16) and (17). The minimum values of $\chi^2_{\min}(\underline{\theta})$ for the fits corresponding to the aforementioned classes of models are expected to follow a χ^2 distribution with ν degrees of freedom (16). Here, $Q(\tau \mid \nu)$ designates the probability of obtaining a fit with a value $\chi^2_{\min}(\underline{\theta})$ greater than τ purely by chance (17). The two-standard deviation confidence limits for the χ^2 distribution correspond to Q values of 0.5 and 99.5%. An excellent fit is expected when $\chi^2_{\min}(\underline{\theta}) \approx \nu$ and for $Q(\chi^2 \mid \nu) \approx 0.5$, whereas $Q(\chi^2 \mid \nu)$ outside the [0.005–0.995] range means that the "fitting model" is not statistically believable.

It is worth mentioning here that there are other statistical tests of "goodness-of-fit." For example, Zhang and Chuang (11), instead of using Q, preferred a test based on the "variance inflation factor" (VIF) to detect if "excess" parameters are involved in a model. The VIF should be less than five for a model to be free of "faked" parameters. Carley and Morgan (18) described a different "goodness of fit" test based on the sign of successive residuals by quantifying the probability of occurrence of strings of residuals of identical signs. The three tests are tantamount for normally distributed errors, which we assume here.

No matter how successful a statistical test is for a given model, if at least one chemical-kinetic criterion is violated then the legitimacy of the scenario put forth becomes suspect (19). Common sense dictates, therefore, that the decision-making process regarding the number of parameters to be used in a model for data representation must include both physical likeliness and statistical goodness-of-fit criteria. Hence, the ultimate model to be retained must fulfill *simultaneously* the conditions

$$\begin{cases} \text{Goodness of fit: } \chi^2_{\min} \approx \nu;\ Q(\chi^2 \mid \nu) \approx 0.5 \\ \text{Physical likeliness: } E_i > 0;\ \Delta H_i < 0;\ S_i < 0. \end{cases} \quad [30]$$

Figures 3a–3c are typical plots of $\chi^2_{\min}$ and $Q(\chi^2 \mid \nu)$, E_i, ΔH_i, and ΔS_i versus the incremental number of parameters from class I–V models in the curve fitting of TOC and

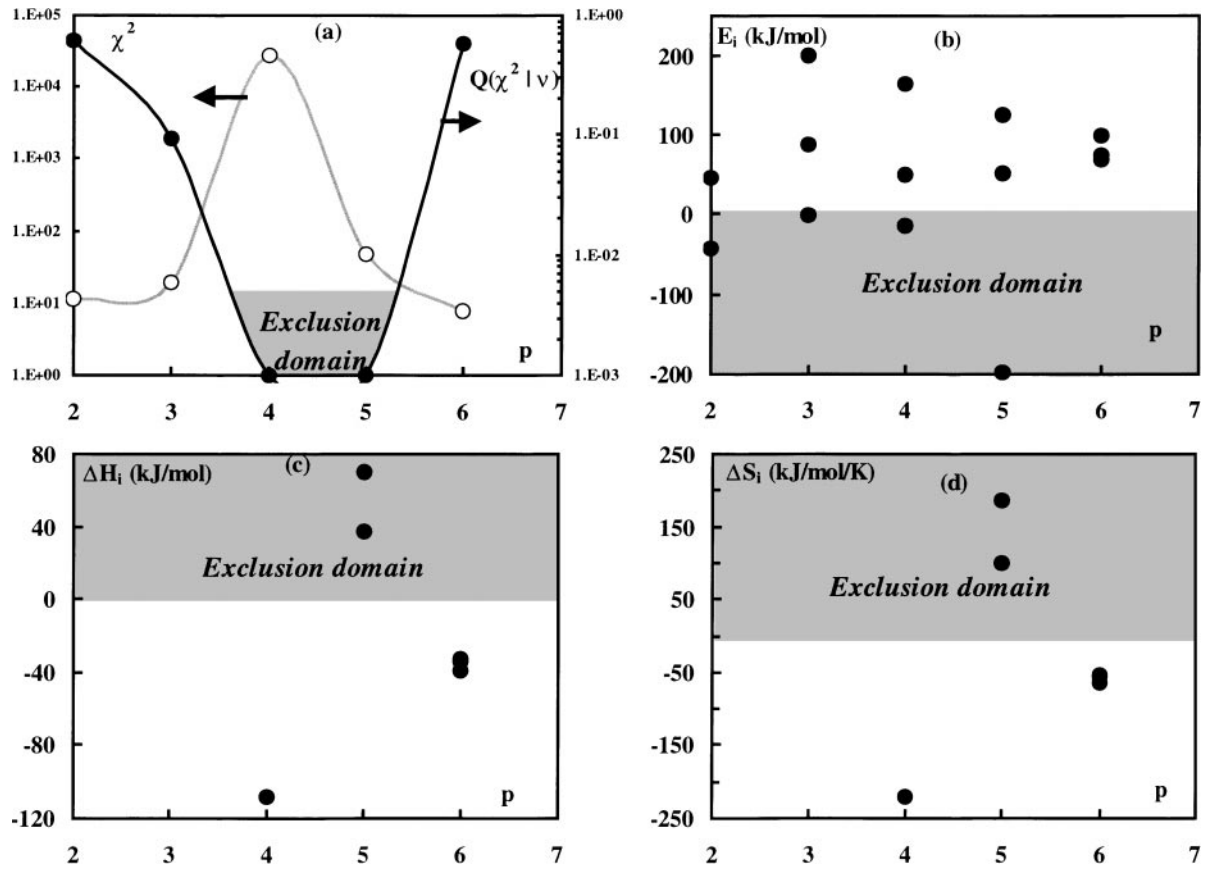

FIG. 3. The $\chi^2_{\min}$, $Q(\chi^2 \mid \nu)$, E_i, ΔH_i, and ΔS_i versus number of parameters used in curve fitting various kinetic models. Model discrimination based on statistical "figure of merit" and physical likeliness.

phenol abatement data of Maugans and Akgerman (20) obtained at 175°C. Similar trends were also observed for all other temperatures and for other data borrowed from the literature and tested in this work (see next section). As can be seen, $\chi^2_{\min}$ and $Q(\chi^2 \mid \nu)$ exhibit bell-shaped variations with increasing numbers of fitted parameters.

Definitely, class III and IV models failed the statistical tests as their Q values fell in the exclusion domain, and also due to their highest $\chi^2_{\min}$. From Fig. 3a, the Q values for the LKM (two parameters), GLKM (three parameters), and ELKM (six parameters) fell inside the statistical acceptance range, with the GLKM slightly disadvantaged with respect to LKM and ELKM. The LKM Q-value was 0.62, that of the GLKM was 0.09, and that of the ELKM was 0.57, the closest to the 0.5 value for an ideal fit. On an exclusive statistical basis, one would obviously choose the LKM, due to its simplicity, for CWO kinetic data representation. Visual inspection of the fits of TOC and phenol carbon, as illustrated in Figs. 4a and 4b, indeed does not permit one to distinguish between the three models, and one would adopt, based on statistical arguments, the simplest class I (or LKM) formulation.

From the physical likeliness standpoint, class III models are to be discarded because of a fitted negative activation energy (Fig. 3b) and an excessively high value for the enthalpy of adsorption (Fig. 3c). Class IV models have some values for the activation energy, the adsorption entropy and enthalpy falling within the exclusion domains. Therefore, class III and IV models should be dismissed because of violation of both criteria in Eq. [30]. The LKM (class I model), the second best choice based on Q statistics, is still unsatisfactory as it provides *unlikely* negative activation energy $E_{AB} = -42.4$ kJ/mol (Fig. 3b). Similarly, the GLKM (class II model) leads to $E_{AC} = -2.0$ kJ/mol, suggesting another form of LKM, i.e., A → B → C. Interestingly, only the six-parameter ELKM provided physically consistent values for adsorption and activation energy parameters (Figs. 2b and 2c) within a range of accepted orders of magnitude for similar reactions reported in the literature.

In summary, this exercise concerning model discrimination emphasizes that selection of kinetic models depends on the nature of the criteria used. Based solely on statistical "figure of merit" criteria, the LKM with the least number of parameters would have been the best choice. Using the more complete set of physical and statistical assessment criteria (Eq. [30]) leads to a different choice, i.e., ELKM. Moreover, it is also possible that by probing a broader population of alternate models, instead of the five outlined in Table 1, could have led to an even different model. However, as shown in the following examples, since EKLM was found to provide physically and statistically sound solutions for a variety of CWO contexts, it would not be justified at this time to develop alternative models.

Illustrative Examples

Selected literature data were used to illustrate the use of ELKM in the CWO of pollutants in wastewaters. The choice of these examples was guided by the need to show that the proposed model and parameter estimation methodology is very general and may be applied to CWO wastewater treatment under a wide variety of conditions (e.g., sub- and supercritical wet oxidation, batch and through-flow kinetic reactors, single- and multiple-pollutant effluents), while monitoring different properties (e.g., TOC, COD, TN). Five scenarios were selected to cover almost all typical contexts that may be encountered.

Example 1—subcritical CWO of phenol in liquid-batch stirred reactor. In this example, Maugans and Akgerman (20) investigated phenol CWO over Pt/TiO_2 catalyst in a

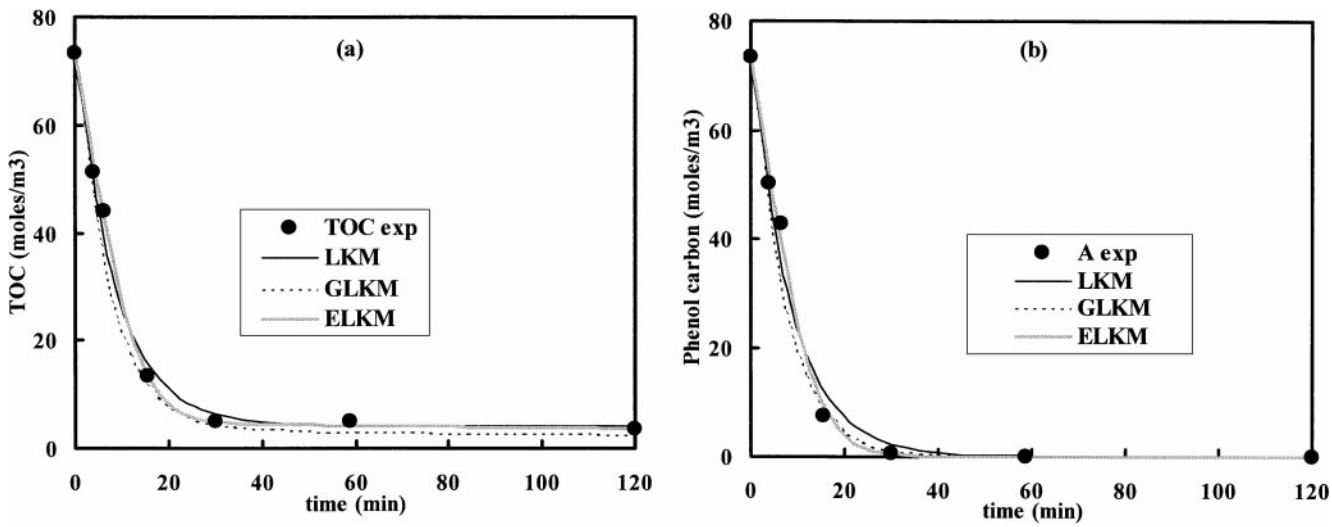

FIG. 4. Prediction by the LKM, GLKM, and ELKM of the TOC and phenolic carbon time decline. Kinetic data from Ref. (20).

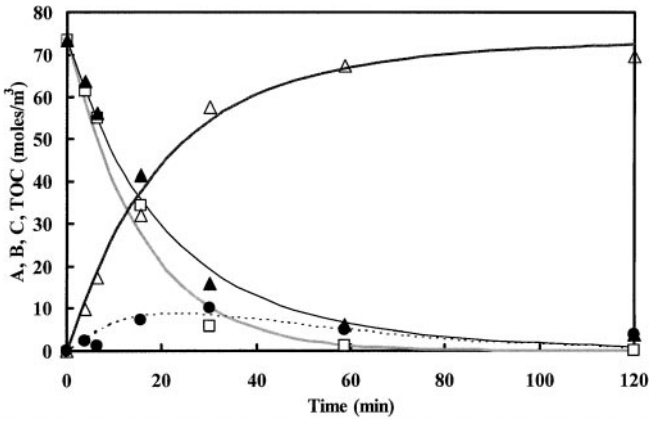

FIG. 5. Predicted and experimental (20) lumped species time profiles of phenol CWO at $T = 165^{\circ}$C. Symbols: ▲, TOC; □, lump A; ●, lump B; △, lump C. Lines show ELKM predicted profiles.

batch stirred reactor in the temperature range 423–473 K using an air pressure and catalyst loading of 4.8 MPa and 2 g/L, respectively. The phenol concentration (A) and TOC (A + B) were the monitored variables.

Typical time-evolution profiles at $T = 438$ K are shown in Fig. 5 in terms of lump A (phenol), B (TOC-A), mineralized carbon (C), and TOC. As seen, the experimental and predicted profiles based on ELKM are in excellent agreement. The Arrhenius and Van't Hoff plots of the obtained controlling step rate constants, $\tilde{k}_{AB}$, $\tilde{k}_{BC}$, and $\tilde{k}_{AC}$, and adsorption equilibrium constants, K_A, K_B, and K_C, are shown in Fig. 6. The vertical bars correspond to the 65% confidence-limit intervals evaluated by the bootstrap method. The apparent activation energies and enthalpies and entropies of adsorption are reported in Table 2 along with their respective standard deviations and the number of experimental data used in the ELKM fit. The values of the obtained apparent activation energies are within the expected range reported in the literature for phenol CWO (20–22). Also the adsorption enthalpies and entropies were found to fulfill the chemical kinetic criteria (15). Finally, the Q values were all within

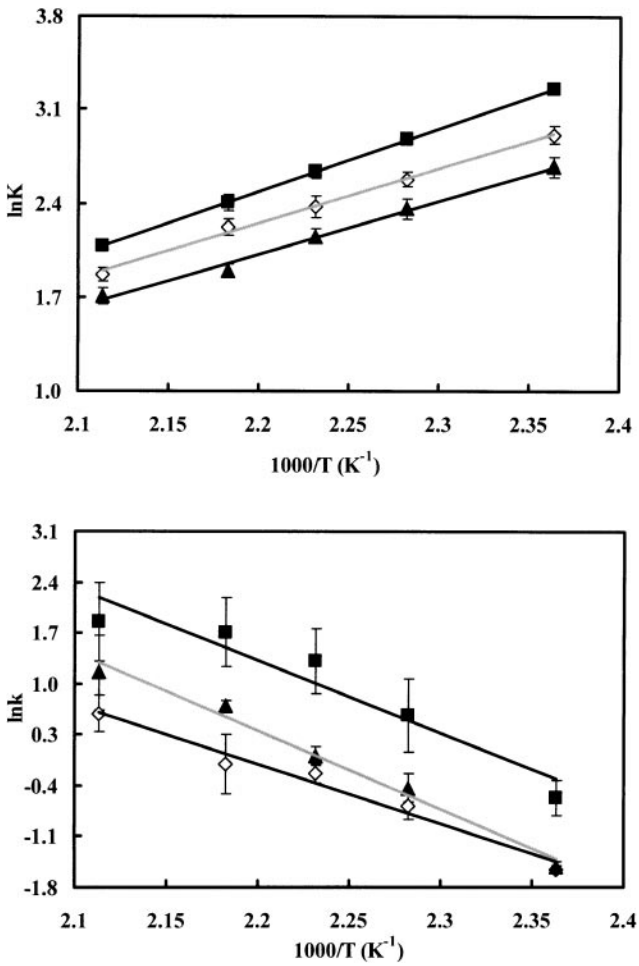

FIG. 6. Van't Hoff and Arrhenius plots for estimated ELKM parameters in Example 1. Symbols: ◇, $\tilde{k}_{AB}$, K_A; ▲, $\tilde{k}_{BC}$, K_B; ■, $\tilde{k}_{AC}$, K_C. Experimental data from (20).

the (0.5–99.5%) acceptance region, confirming that the estimated parameters are highly reliable.

Example 2—subcritical CWO of softwood Kraft pulp mill effluent in liquid-batch stirred reactor. In this example,

TABLE 2

ELKM Kinetic Parameters for Example 1

Constant	$\Delta S \times 10^3$ (kJ mol^{-1} K^{-1})	ΔH (kJ mol^{-1})	$\sigma_{\Delta S} \times 10^3$ (kJ mol^{-1} K^{-1})	$\sigma_{\Delta H}$ (kJ mol^{-1})	χ^2	Q
K_A	−56.5	−34.1	2.8	1.3	3.1	0.59
K_B	−55.8	−32.9	3.3	1.5	4.9	0.31
K_C	−65.2	−39.0	1.6	0.7	0.03	0.99
	$\tilde{k}_{io}$	E (kJ mol^{-1})	$\sigma_{\tilde{k}_{io}}$	σ_E (kJ mol^{-1})	χ^2	Q
$\tilde{k}_{AB}$	5.96E+07	67.5	13.4	6.0	3.7	0.49
$\tilde{k}_{BC}$	2.84E+11	97.5	14.7	6.7	4.4	0.39
$\tilde{k}_{AC}$	1.22E+09	73.5	32.4	14.6	3.7	0.50
$n \times m$	7[(TOC data) + (A data)] × 5(temperature) = 70 experimental data					

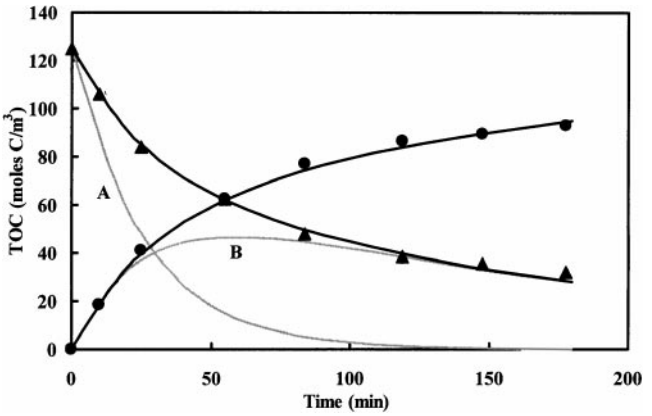

FIG. 7. Predicted and experimental (10) lumped carbon species profiles of the CWO of softwood Kraft pulp mill effluent. Symbols: ▲, TOC; ●, lump C. Lines show ELKM predicted profiles of A, B, C, TOC.

Zhang and Chuang (10, 11) monitored TOC during the CWO of a softwood Kraft pulp mill effluent. The black liquor was contacted with Pt–Pd–Ce/alumina catalyst in a batch slurry reactor in the temperature range 433–463 K, with O_2 pressure of 1.5 MPa, catalyst loading of 8.3 g/L, and initial liquor TOC 1500 mg/L. Application of GLKM by Zhang and Chuang (10) to their own data led to computed activation energies of 66.1, 160.8, and 981.5 kJ/mol for k_1, k_2, and k_3, respectively. Visibly, the activation energy associated with k_3 is unrealistically high.

Figure 7 shows ELKM predictions versus measured TOC (A + B lumps), deduced off-liquor lump C, and simulated A and B lump profiles at 463 K. Similar good quality fits were obtained for data at different temperatures. The apparent activation energies and enthalpies and entropies of adsorption are tabulated in Table 3, and the Arrhenius and Van't Hoff plots are shown in Fig. 8. The Q values of the fitted parameters were in excess of the 0.5% threshold.

Example 3—subcritical CWO of a petrochemical effluent in liquid-batch stirred reactor. This example dealing with the disappearance of polluting species as monitored by COD was selected with the aim of generalizing the proposed ELKM to industrial effluents. COD is an overall variable which reflects all chemical entities of organic and/or

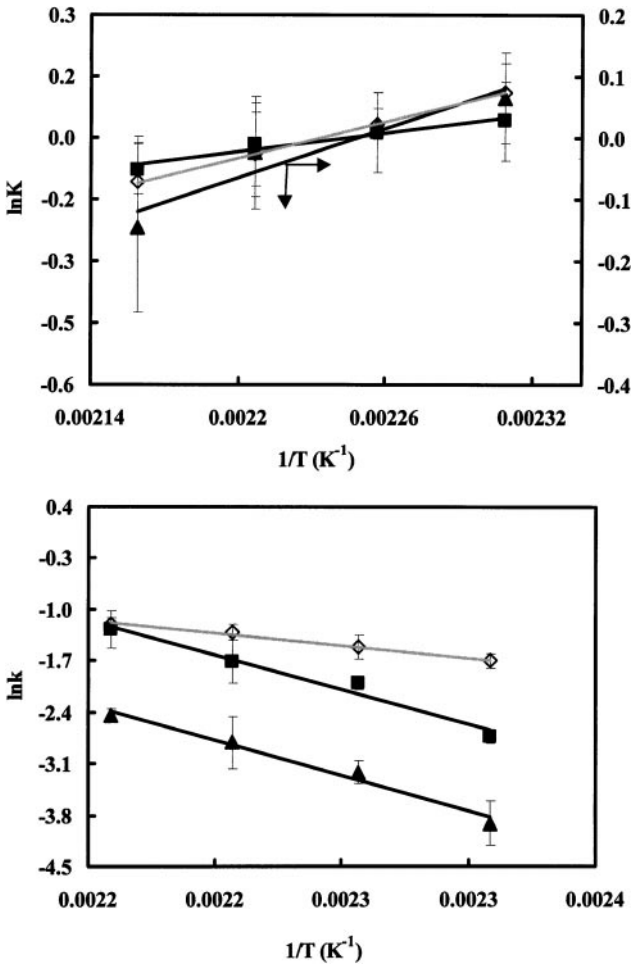

FIG. 8. Van't Hoff and Arrhenius plots for estimated ELKM parameters in example 2. Symbols: ◇, $\tilde{k}_{AB}$, K_A; ▲, $\tilde{k}_{BC}$, K_B; ■, $\tilde{k}_{AC}$, K_C. Experimental data from (10).

TABLE 3

ELKM Kinetic Parameters for Example 2

Constant	$\Delta S \times 10^3$ (kJ mol^{-1} K^{-1})	ΔH (kJ mol^{-1})	$\sigma_{\Delta S} \times 10^3$ (kJ mol^{-1} K^{-1})	$\sigma_{\Delta H}$ (kJ mol^{-1})	χ^2	Q
K_A	−27.5	−12.3	0.8	0.3	0.2	0.98
K_B	−10.7	−4.8	1.2	0.5	1.2	0.81
K_C	−26.0	−11.6	5.4	2.4	2.2	0.59
	$\tilde{k}_{io}$	E (kJ mol^{-1})	$\sigma\tilde{k}_{io}$	σ_E (kJ mol^{-1})	χ^2	Q
$\tilde{k}_{AB}$	462.48	28.1	8.1	3.6	0.7	0.90
$\tilde{k}_{BC}$	5.97E+06	69.1	14.9	6.8	1.0	0.84
$\tilde{k}_{AC}$	1.17E+09	84.6	19.1	8.4	2.0	0.63
$n \times m$	8(TOC data) × 4(temperature) = 32 experimental data					

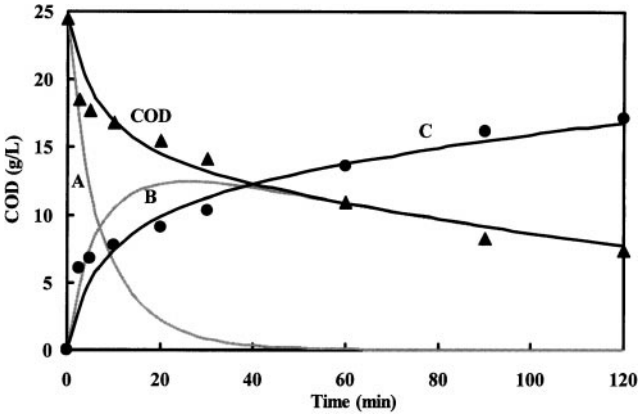

FIG. 9. Predicted and experimental (9) COD profile of the CWO of a petrochemical effluent. Symbols: ▲, COD; ●, lump C. Lines show ELKM predicted profiles of A, B, C, and COD.

inorganic nature, susceptible to oxidization. Being a lumped variable, COD is an indirect descriptor of soluble pollutants when complex heteroatom-containing wastewaters have to be treated by CWO, and hence it can be suitable for the proposed lumping strategy. A representative example is borrowed from Lin *et al.* (9), who studied the kinetics and performance of the CWO of highly polluted petrochemical plant wastewater. The treatment was conducted using ZnO catalyst loaded at 500 mg/L in a liquid-batch stirred reactor supplied with air at temperatures 473, 498, and 513 K. Here also, Lin *et al.* (9) reported an abnormal behavior of GLKM despite the excellent fit of their COD data. Indeed, the rate constant k_3 exhibited unrealistic temperature dependence with negative activation energy.

Figures 9 and 10 and Table 4 summarize the ELKM fit performance, the kinetic parameter values, and confidence intervals using Lin *et al.*'s (9) kinetic data. All of the fitted constants fulfilled the chemical kinetic (15) and statistical (Q test) criteria.

Example 4—subcritical CWO of β-alanine and aniline in liquid-batch stirred reactor. Deiber *et al.* (23) investigated the CWO conversion of organic nitrogen-containing aqueous wastes (N-Org) into ammonia and other nitrogen-bearing end-products (N_2, NO_2, NO_3^-). Different substrates were used, including 4-nitrophenol

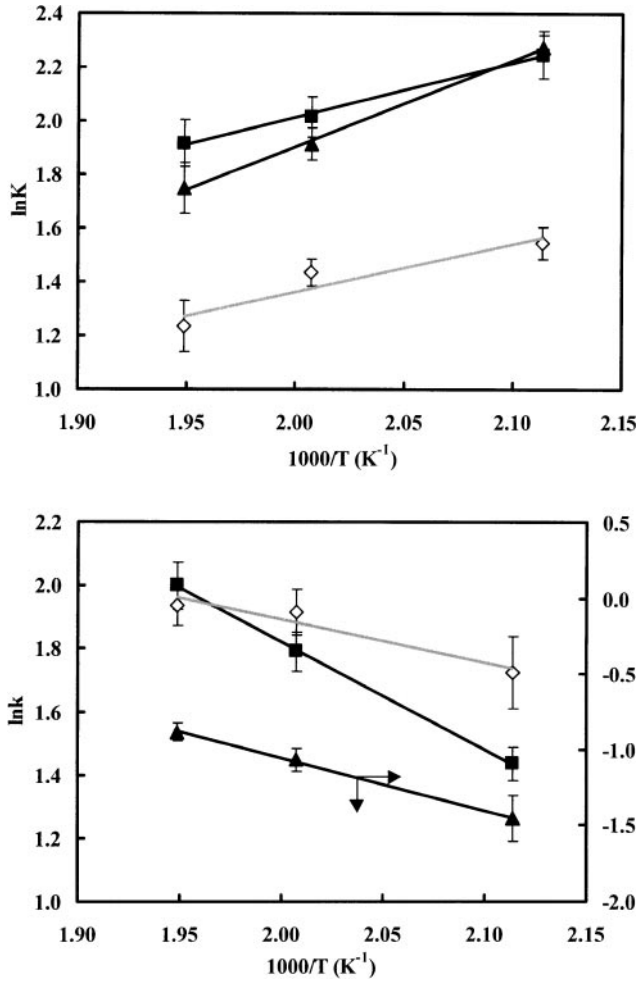

FIG. 10. Van't Hoff and Arrhenius plots for estimated ELKM parameters in Example 3. Symbols: ◇, $\tilde{k}_{AB}$, K_A; ▲, $\tilde{k}_{BC}$, K_B; ■, $\tilde{k}_{AC}$, K_C. Experimental data from (9).

TABLE 4

ELKM Kinetic Parameters for Example 3

Constant	$\Delta S \times 10^3$ (kJ mol^{-1} K^{-1})	ΔH (kJ mol^{-1})	$\sigma_{\Delta S} \times 10^3$ (kJ mol^{-1} K^{-1})	$\sigma_{\Delta H}$ (kJ mol^{-1})	χ^2	Q
K_A	−23.9	−17.6	7.1	3.6	2.3	0.33
K_B	−38.6	−27.2	4.4	2.2	0.2	0.93
K_C	−17.2	−16.9	5.3	2.6	0.2	0.95
	$\tilde{k}_{io}$	E (kJ mol^{-1})	$\sigma\tilde{k}_{io}$	σ_E (kJ mol^{-1})	χ^2	Q
$\tilde{k}_{AB}$	76.5	10.1	6.4	3.2	1.4	0.56
$\tilde{k}_{BC}$	301.0	28.0	7.6	3.8	0.2	0.96
$\tilde{k}_{AC}$	5593.5	28.2	4.3	2.1	0.1	0.98
$n \times m$	9(TOC data) × 3(temperature) = 27 experimental data					

(nitro-compound), β-alanine (amino acid), aniline (amino-aromatics), and ammonia (inorganic compound). The examples given below were limited to the CWO of β-alanine and aniline aqueous solutions over Mn/Ce mixed oxide catalyst (2–8 g/L) at 533 K. Deiber *et al.* (23) modified the GLKM (5) by including a step for the interactions between N-Org species and the catalyst. The derived model led to unrealistic fractional orders for catalyst concentrations and rate constant functions of catalyst concentration.

To validate the ELKM on nitrogenous wastewater effluents, only the fate of nitrogen was described kinetically using three lumps: A for the parent compounds (N-Org: β-alanine or aniline), B for ammonia (N–NH_3, the recalcitrant species, (24)), and C for end products such as N_2 and other unidentified species. Typical results of predicted profiles along with experimental values of the nitrogen lumps for aniline and β-alanine are shown in Figs. 11a and 11b. Table 5 summarizes the estimated parameters for β-alanine and aniline CWO treatment. In the case of aniline, kinetic tests were available for two different catalyst loadings. The ELKM kinetic parameters obtained using the two data sets separately compare very well, showing that they are indeed independent from the catalyst loading.

Example 5—supercritical CWO of phenol in a fixed bed reactor. This example deals with experimental data on supercritical wet oxidation (SCWO) of phenol over a transition-metal oxide catalyst in an integral fixed-bed reactor (25). Three initial phenol concentrations ranging from 3.76×10^{-4} to 1.18×10^{-3} mol/L were used at 673 K under a total pressure of 240 bar and an initial molar ratio O_2/phenol = 56. Phenol concentration and TOC in the exit stream were monitored under steady-state conditions for different phenol inlet molar rates. The difference between TOC and phenol concentration was due to the occurrence of water-dissolved intermediate products formed during the reaction. Earlier attempts to describe the kinetics of phenol degradation under supercritical conditions in a continuous reactor failed to offer a complete picture of the process. Krajnc and Levec (25) used power-law expressions and treated separately and independently the TOC and the phenol degradation kinetics. A LHHW approach was also attempted (25), but with little success.

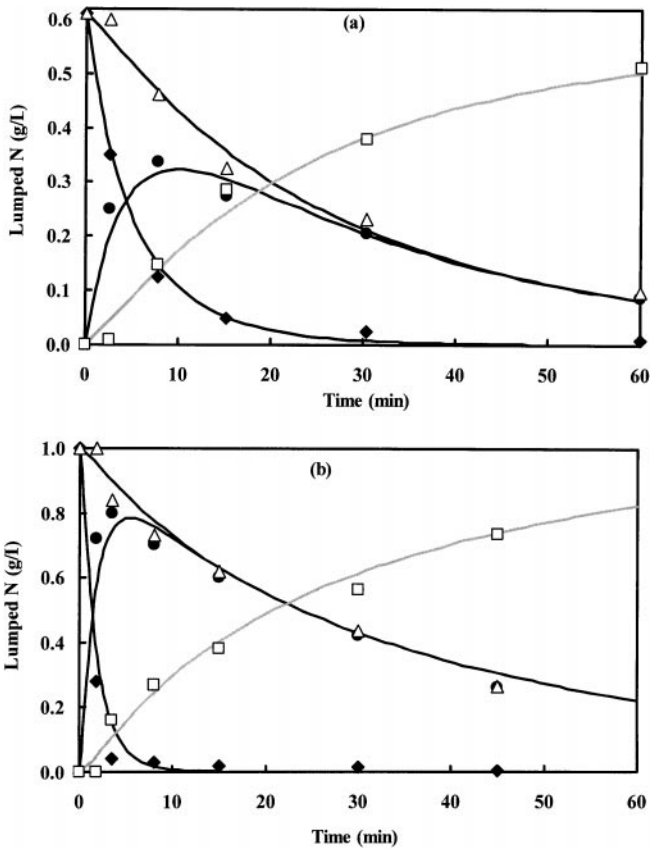

FIG. 11. Predicted and experimental (23) profiles of lumped nitrogenous species, (a) aniline and (b) β-alanine CWO. Symbols: ◆, N-Org (lump A); ●, N-NH_3 (lump B); □, lump C; △, TN. Lines show ELKM predicted profiles of A, B, C, TN.

By means of the proposed ELKM, the TOC and phenol concentrations downstream of the SCWO reactor were evaluated by integrating, with respect to residence time, the ODE system Eqs. [14]–[16] and were compared with actual

TABLE 5

ELKM Kinetic Parameters for Example 4

Pollutant	Observation	$\tilde{k}_{AB}$	$\tilde{k}_{BC}$	$\tilde{k}_{AC}$	K_A	K_B	K_C
Aniline	[Cat] = 2 g/L	0.13	0.0067	0.014	0.29	2.14	0.43
	[Cat] = 8 g/L	0.14	0.0078	0.013	0.29	2.14	0.43
	average	0.13	0.0073	0.014	0.29	2.14	0.43
	σ	0.005	0.0004	0.002	0.01	0.01	0.01
$n \times m$	[6(N-NH_3 data) + 6(N-organic data)] × 2([catalyst loading]) = 24 experimental data per temperature						
β-Aniline	[Cat] = 4 g/L	0.47	0.037	0.017	0.41	2.06	0.40
	σ	0.01	0.001	0.001	0.01	0.01	0.01
$n \times$ m	8(N-NH_3 data) + 8(N-organic data) = 16 experimental data per temperature						

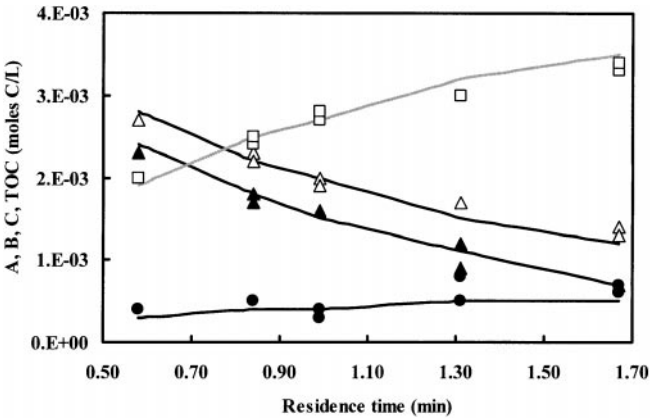

FIG. 12. Predicted and experimental time-on-stream profiles of phenol SCWO. Symbols: ▲, lump A; △, TOC; ●, lump B; □, lump C. Lines show ELKM predicted profiles. Experimental data from (25).

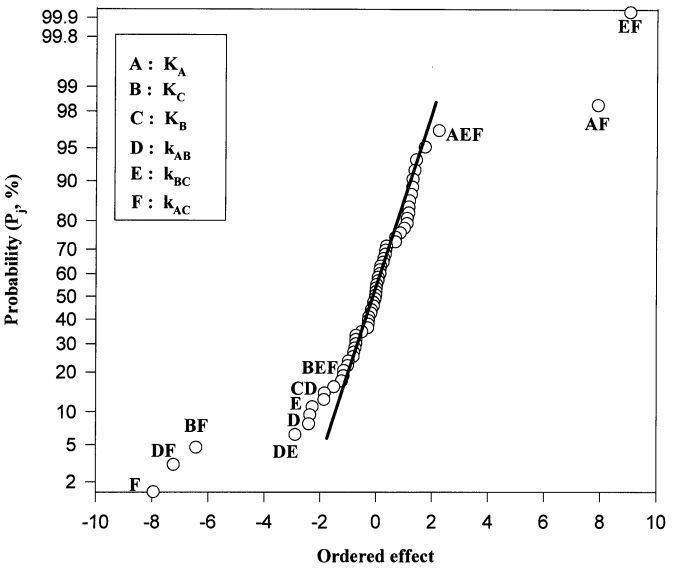

FIG. 13. Full 2^6 factorial design for parameter effects.

measurements at the reactor outlet. The lumps were defined in the same manner as in example 1. Comparison between predictions and experimental data is shown in Fig. 12 for an inlet phenol concentration of 7.9×10^{-4} mol/L. Table 6 is a summary of the estimated parameters for the three inlet phenol concentrations. It is worth mentioning that ELKM is the first model capable of describing simultaneously the fate of phenol, its break-down water-dissolved organic intermediates (TOC—residual phenol), and the end products generated under catalytic SCWO conditions. As in example 4, the kinetic parameters were calculated for each phenol inlet concentration; it is comforting to notice the parameter consistency for each inlet concentration, indicating that as expected, these are independent from the phenol inlet concentration. Moreover, the standard deviations of fitted parameters calculated from either the three replicated experiments or the "bootstrap" method are essentially coincident. This provides strong support for using the bootstrap method to assess the confidence intervals of parameters for unreplicated kinetic experiments. This is also indicative of the robustness of ELKM by providing highly reliable $\tilde{k}_i$ and K_i constants.

ELKM "Proof-of-Concept"

Despite the encouraging results in the five previous examples corresponding to a wide selection of experimental conditions, the above-fitted parameters and the conclusions drawn are valid only if the proposed model is shown to be statistically robust and reasonably sensitive to all of its fitted kinetic parameters. To this end, a series of simulations was carried out with the model in which each parameter in the set $\tilde{k}_{AB}, \tilde{k}_{BC}, \tilde{k}_{AC}, K_A, K_B$, and K_C was perturbed within ±20% around the optimized set $\underline{\theta}$. For each combination of "perturbed" parameters, the quadratic criterion, $\chi^2(\underline{\theta})$, was re-evaluated. A two-level unreplicated 2^6 factorial design (26) was then established to analyze the ELKM sensitivity to the six fitted parameters. The normal probability plot of ordered effects calculated using the data of example 2 is illustrated in Fig. 13. It is seen that the statistically negligible effects are normally distributed with a mean zero and variance σ^2, and they tend to fall along a straight line. The dominant effects, in contrast,

TABLE 6

ELKM Kinetic Parameters for Example 5

Observations	$\tilde{k}_{AB}$	$\tilde{k}_{BC}$	$\tilde{k}_{AC}$	K_A	K_B	K_C
$C_{phenol,o} = 3.76 \times 10^{-4}$ mol/L	0.21	0.29	0.84	1.11	1.00	0.98
$C_{phenol,o} = 7.84 \times 10^{-4}$ mol/L	0.18	0.36	0.88	1.20	1.00	1.00
$C_{phenol,o} = 1.18 \times 10^{-4}$ mol/L	0.27	0.36	0.93	1.25	1.00	1.01
Average	0.22	0.36	0.90	1.22	1.00	1.01
σ_i[a]	0.05	0.043	0.046	0.068	0.01	0.014
σ	0.03	0.029	0.036	0.043	0.01	0.02
$n \times m$	[8(TOC data) + 8(phenol data)] × 3(initial [phenol]) = 48 experimental data per temperature					

[a] Standard deviation between kinetic constants for the three different initial concentrations of phenol.

exhibit non-zero means and *do not lie* along that line. This proves that their contribution impacts significantly the kinetic model response in the quadratic criterion $\chi^2(\underline{\theta})$. This was the case for the main effects of $\tilde{k}_{AC}$, $\tilde{k}_{AB}$, and $\tilde{k}_{BC}$ and the second-order effects of $\tilde{k}_{AB}\tilde{k}_{AC}$, $K_C\tilde{k}_{AC}$, $\tilde{k}_{AB}\tilde{k}_{BC}$, $K_B\tilde{k}_{AB}$, $K_A\tilde{k}_{AC}$, and $\tilde{k}_{AC}\tilde{k}_{BC}$. The third- fourth-order effects were found to be marginal. Based on Fig. 13, it may be concluded that the effects of all six fitted kinetic and equilibrium parameters are statistically significant. The same conclusions apply for the other four illustrative examples.

ELKM Parameters Joint-Confidence Region Analysis

To evaluate the uncertainty on the kinetic parameters, the bootstrap method described earlier can also be used to estimate the joint-confidence regions. For illustration, the joint-confidence regions for example 4 will be discussed. The $B = 50$ bootstrap sets P_b^* were re-sampled from the measured data of aniline wet oxidation. The covariance matrix calculated by Eq. [23] is

$$\underline{\underline{M}} \times 10^4 = \begin{bmatrix} 0.5604 & 0.0446 & -0.0206 & 0.2763 & 0.0155 & -0.0049 \\ 0.0446 & 0.0433 & 0.0074 & 0.0342 & 0.0012 & -0.0270 \\ -0.0206 & 0.0074 & 0.1833 & -0.0513 & 0.0015 & 0.0094 \\ 0.2763 & 0.0342 & -0.0513 & 0.2481 & 0.0181 & -0.0063 \\ 0.0155 & 0.0012 & 0.0015 & 0.0181 & 0.0023 & 0.0055 \\ -0.0049 & 0.0270 & 0.0094 & -0.0063 & 0.0055 & 0.0576 \end{bmatrix}. \quad [31]$$

The diagonal elements are the estimated bootstrap variances of vector $\underline{\theta}$ reported in Table 5. The off-diagonal elements designate the various two-parameter covariances. In this example, the size of the confidence region $\Pi_1^p \sqrt{\lambda_i}$ was equal to 4×10^{-17}, where λ_i are the eigenvalues associated to with matrix M. This confirms the good precision in the estimated vector $\underline{\theta}$. For the same example, the correlation matrix, Eq. [24],

$$\Omega = \begin{array}{c} \begin{matrix} K_A & K_B & K_C & \tilde{k}_{AB} & \tilde{k}_{BC} & \tilde{k}_{AC} \end{matrix} \\ \begin{bmatrix} 1.0 & & & & & \\ 0.3 & 1.0 & & & & \\ -0.1 & 0.1 & 1.0 & & & \\ 0.7 & 0.3 & -0.2 & 1.0 & & \\ 0.4 & 0.1 & 0.1 & 0.7 & 1.0 & \\ 0.0 & -0.5 & 0.1 & -0.1 & 0.5 & 1.0 \end{bmatrix} \end{array} \begin{matrix} K_A \\ K_B \\ K_C \\ \tilde{k}_{AB} \\ \tilde{k}_{BC} \\ \tilde{k}_{AC} \end{matrix} \quad [32]$$

indicates that the estimated parameters are weakly cross-correlated to each other. Therefore, the significance of the fitted parameters does not deteriorate when the ELKM adsorption and kinetic constants are evaluated simultaneously.

CONCLUSION

Direct use of the generalized lumped kinetic model of Li *et al.* (5) for solid-catalyzed wet oxidation (CWO) often leads to kinetic parameters with no physical meaning. Instead, a versatile extended lumped kinetic model (ELKM) involving characteristic features of heterogeneous processes, i.e., adsorption/desorption and surface reactions, was proposed within the Langmuir–Hinshelwood–Hougen–Watson framework. ELKM uses a three-lump triangular scheme. For the proposed ELKM to be as widely applicable as possible, the lumps were defined in very general terms as follows: (i) a lump for parent compounds, (ii) a lump for the water-dissolved breakdown intermediate compounds, (iii) and a lump for off-solution gas and solid end products. The ELKM's versatility was illustrated using five different contexts of CWO operations. This included CWO of single contaminants and complex broths as well as batch and through-flow reactors in sub- and supercritical conditions. The model was shown to be statistically robust and capable of predicting the time profiles of the various lumps involved in heterogeneous CWO as well as the kinetic and the adsorption/desorption equilibrium parameters.

APPENDIX: NOMENCLATURE

B	bootstrap replication number
C	concentration (mol/m^3)or (g/L)
E	activation energy (kJ/mol)
k	controlling-step rate constant (min^{-1})
$\tilde{k}$	embedded rate constant (mol kg^{-1} cat min^{-1} for concentrations in mol/m^3)
$\tilde{k}_{io}$	Arrhenius pre-exponential factor (mol kg^{-1} cat min^{-1}; concentrations in mol/m^3)
K	adsorption equilibrium constant (m^3/mol for concentrations in mol/m^3)
m_{cat}	catalyst loading (kg cat/m^3)
m	number of monitored state variables
$\underline{\underline{M}}$	covariance matrix
n	number of runs in P set
p	dimension of vector $\underline{\theta}$
P	kinetic data set
R	catalytic reaction rate (mol g^{-1} cat min^{-1} for concentrations in mol/m^3)
Q	goodness-of-fit probability function
t	time (min)
T	temperature (K)
U	least-squares problem
U_L	liquid superficial velocity (m/min)
X	active site concentration (mol/kg cat)
Y	ELKM state variable, C_A, C_B, TOC, etc.
z	catalyst bed length (m)

Greek Letters

τ	residence time (min)
ΔH	adsorption enthalpy (kJ/mol)
ΔS	adsorption entropy (kJ mol^{-1} K^{-1})
$\underline{\theta}$	ELKM parameters vector
$\underline{\tilde{\theta}}$	estimated parameters vector in bootstrap replication
$\chi^2(\theta)$	"unweighted least-squares" criterion, Eq. [19]
σ	standard error
$\underline{\underline{\Omega}}$	correlation matrix
χ^2	chi-square merit function
λ	eigenvalue

Sub- and Superscripts

A, B, C	chemical lumps
b	bootstrap
cat	catalyst
i	index of experimental run
*	catalyst site; bootstrap replication
o	initial
—	predicted by model
$\langle\,\rangle$	ensemble-average operator

Abbreviations

cov	covariance
CWO	(solid-) catalyzed wet oxidation
ELKM	extended lumped kinetic model
GLKM	generalized lumped kinetic model
LHHW	Langmuir–Hinshelwood–Hougen–Watson
LKA	lumped kinetic approach
LKM	lumped kinetic model
SCWO	supercritical wet oxidation
TOC	total organic carbon
COD	chemical oxygen demand
TN	total nitrogen
TX	total halogen
TP	total phosphorus
TS	total sulfur

REFERENCES

1. Sheldon, R. A., *J. Chem. Tech. Biotechnol.* **68**, 381 (1997).
2. Meunier, B., and Sorokin, A., *Acc. Chem. Res.* **30**, 470 (1997).
3. Weekman, V. W., Jr., *AIChE Symp. Ser.* **75**(11), 3 (1979).
4. Li, L., Crain, N., and Gloyna, E. F., *Water Env. Res.* **68**(5), 841 (1996).
5. Li, L., Chen, P., and Gloyna, E. F., *AIChE J.* **37**(11), 1687 (1991).
6. Ploos Van Amstel, J. J. A., and Rietema, K., *Chem. Ing. Technol.* **45**, 1205 (1973).
7. Baillod, C. R., Faith, B. M., and Masi, O., *Environ. Prog.* **1**(3), 217 (1982).
8. Foussard, J. N., Delbellefontaine, H., and Besombse-Vailhe, J., *J. Environ. Eng.* **115**(2), 367 (1989).
9. Lin, S. H., Ho, S. J., and Wu, C. L., *Ind. Eng. Chem. Res.* **35**, 307 (1996).
10. Zhang, Q., and Chuang, K. T., *Appl. Cata. B Environ.* **17**, 321 (1998).
11. Zhang, Q., and Chuang, K. T., *AIChE J.* **45**, 145 (1999).
12. Press, H. W., Teukolsly, S. A., Vetterling, W. T., and Flannery, B. P., "Numerical Recipes, The Art of Scientific Computing," 2nd ed. Cambridge Univ. Press, Cambridge, UK, 1992.
13. Efron, B., and Tibshirani, R., *Stat. Sci.* **1**, 54 (1986).
14. Efron, B., and Tibshirani, R., "An Introduction to the Bootstrap." Chapman & Hall, London, 1993.
15. Boudart, M., Mears, D., and Vannice, M. A., *Ind. Chim. Belge* **32**, 281 (1967).
16. Cumpson, P. J., and Seah, M. P., *Surf. Interface Anal.* **18**, 345 (1992).
17. Gengenbach, T. R., Chatelier, R. C., and Griesser, H. J., *Surf. Interface Anal.* **24**, 271 (1996).
18. Carley, A. F., and Morgan, P. H., "Computational Methods in the Chemical Sciences." Ellis Horwood, Chichester, 1989.
19. Carberry, J. J., "Chemical and Catalytic Reaction Engineering." McGraw–Hill, New York, 1976.
20. Maugans, C. B., and Akgerman, A., *Water Res.* **31**(12), 3116 (1997).
21. Pintar, A., and Levec, J., *J. Catal.* **135**, 345 (1992).
22. Atwater, J. E., Akse, J. R., McKinnis, J. A., and Thompson, J. O., *Chemosphere* **34**, 203 (1997).
23. Deiber, G., Foussard, J. N., and Debellefontaine, H., *Environ. Poll.* **96**(3), 311 (1997).
24. Webley, P. A., Tester, J. W., and Holgate, H. R., *Ind. Eng. Chem. Res.* **30**, 1745 (1991).
25. Krajnc, M., and Levec, J., *Ind. Eng. Chem. Res.* **36**, 3439 (1997).
26. Montgomery, D. C., "Design and Analysis of Experiments," 3rd ed. Wiley, New York, 1991.